Available online at www.sciencedirect.com
ScienceDirect
Journal of Asian Earth Sciences 29 (2007) 320–335
Journal of Asian Earth Sciences
www.elsevier.com/locate/jaes

Petrogenesis of volcanic rocks in the Sangxiu Formation, central segment of Tethyan Himalaya: A probable example of plume–lithosphere interaction

Dicheng Zhu [a,*], Guitang Pan [a], Xuanxue Mo [b], Zhongli Liao [a], Xinsheng Jiang [a], Liquan Wang [a], Zhidan Zhao [b]

[a] *Chengdu Institute of Geology and Mineral Resources, 610082 Chengdu, China*
[b] *China University of Geosciences, 100083 Beijing, China*

Received 16 December 2004; accepted 14 December 2005

Abstract

The ∼133 Ma volcanic rocks of Sangxiu Formation are distributed in the eastern part of the central Tethyan Himalaya and belong paleogeographically to the northeastern margin of Greater India. These volcanic rocks include alkaline basalts and felsic volcanic rocks. Major and trace element abundances and whole-rock isotopic data for selected samples of these volcanic rocks are used to infer their petrogenesis. Geochemically, the Sangxiu basalts are closely similar to the Emeishan high-Ti basalts. Major and trace element data and Sr–Nd isotopic compositions suggest that the Sangxiu basalts may have been derived from an OIB-type mantle source, with discernable contributions from subcontinental lithospheric mantle (SCLM). The basaltic magmas may have formed as a result of the infiltration of plume-derived melts into the base of the lithosphere in a continental rift setting. The Sangxiu felsic volcanic rocks share most of the geochemical features of A-type granite, and have Sr–Nd isotopic compositions which differ considerably from the Sangxiu basalts, suggesting that they originated from the anatexis of ensialic continental crust. The Sangxiu volcanic rocks may be considered as the consequence of an interaction between the Kerguelen hotspot and the lithosphere of the northeastern margin of Greater India at ∼133 Ma, and may represent the initial stage of the separation of Greater India from southwestern Australia.

Keywords: Petrogenesis; Volcanic rocks; Sangxiu Formation; Tethyan Himalaya

1. Introduction

The Tethyan Himalaya is located between the Indus–Yarlung Zangbo Suture Zone to the north and Higher Himalayan crystalline assemblages to the south. It belongs paleogeographically to the northern margin of 'Greater India'. The Sangxiu Formation occurs in the central segment of the Tethyan Himalaya. It comprises interbedded volcano-sedimentary strata, varying in age from Late Jurassic to Early Cretaceous (Zhong et al., 2003). The sedimentary strata are characterized by coarse to fine-grain quartz sandstone, quartz greywacke, siltstone and shales. The volcanic rocks include both basaltic and felsic varieties. The petrography and mineralogy of these volcanic rocks have been reported previously (Team of Integrated General Investigation, 1979; Bureau of Geology and Mineral Resources of Xizang Autonomous Region, 1993; Team of Regional Geological Survey, 1994; Zhong et al., 2003), but little has been done on the geochemistry and petrogenesis of these volcanic rocks.

These volcanic rocks are worthy of further study for several reasons: 1). They are distributed in an area of 200 km×50 km, southeast of Yangzuoyong Co, along the eastern part of the central Tethyan Himalaya (Fig. 1a); 2). They are interestingly aligned with the northward extension of the Ninetyeast Ridge in the

* Corresponding author. Tel.: +86 28 83232525; fax: +86 28 83222657.
E-mail address: cdzdc@cgs.gov.cn (D.C. Zhu).

1367-9120/$ - see front matter © 2006 Elsevier Ltd. All rights reserved.
doi:10.1016/j.jseaes.2005.12.004

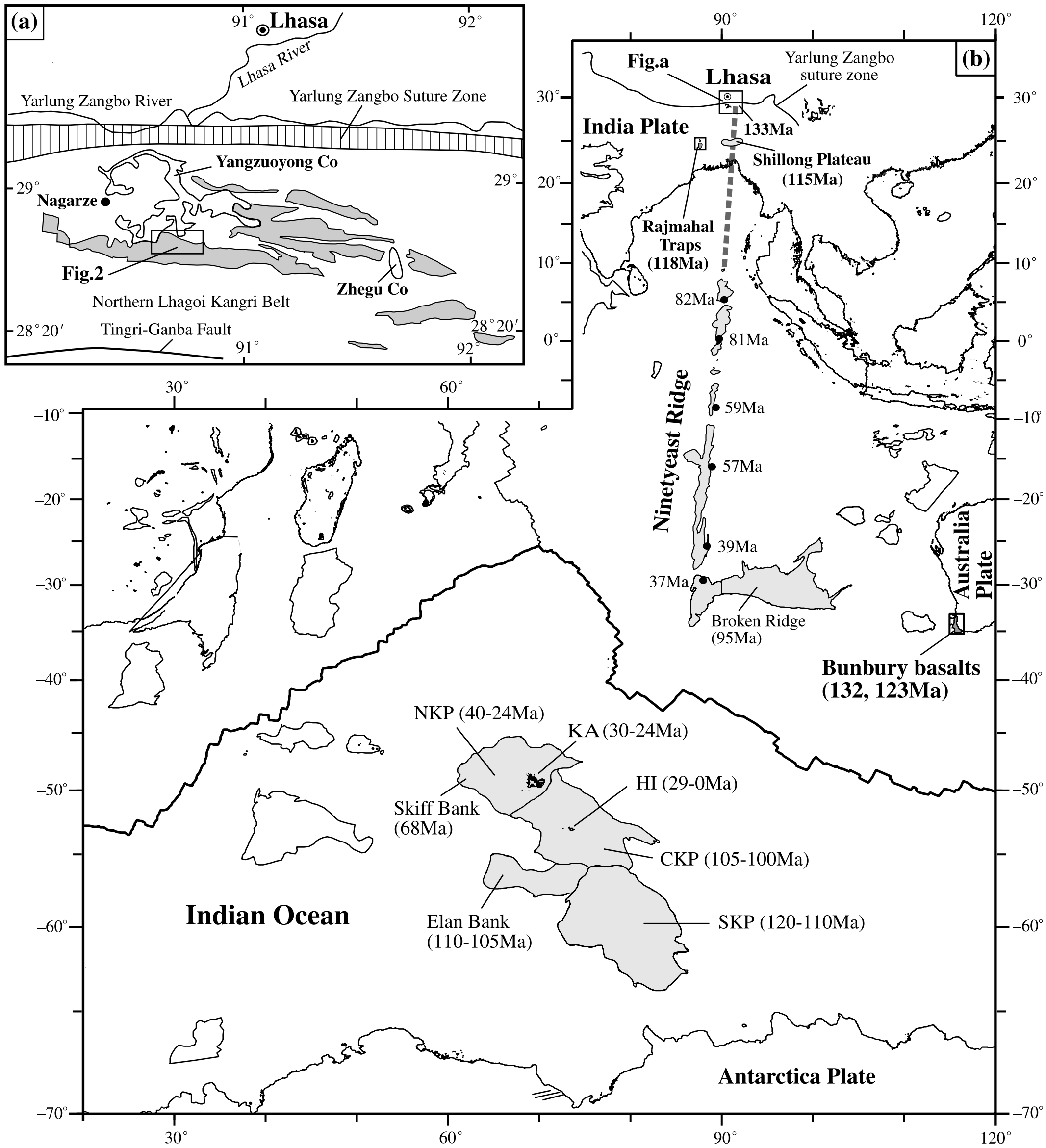

Fig. 1. (a) Distribution of the Sangxiu volcanic rocks in the central segment of Tethyan Himalaya (in gray, Pan et al., 2004). (b) Physiographic map of the Indian Ocean and surrounding continents, showing spatial-temporal locations of the Sangxiu volcanic rocks and products related to the Kerguelen plume (including the various provinces: Southern Kerguelen Plateau (SKP), Central Kerguelen Plateau (CKP), Northern Kerguelen Plateau (NKP), Elan Bank and Skiff Bank, Broken Ridge and Ninetyeast Ridge, Kerguelen Archipelago (KA), Heard and MacDonald Island (HI), Ingle et al., 2003). Locations for continental tholeiites on the margins of eastern India (Rajmahal Traps) and southwestern Australia (Bunbury basalts) are also illustrated (Ingle et al., 2003); these may be related to Kerguelen plume activity (Frey et al., 1996; Ingle et al., 2002a). Age-constraints for various provinces and continental volcanics are from Coffin et al. (2002), Duncan (2002) and Zhu et al. (2005). Note that the Sangxiu volcanic rocks align well with the northward extension of the Ninetyeast Ridge; the dashed gray line illustrates the possible track of Kerguelen hotspot.

Indian Ocean (Fig. 1b); and 3). The age of 133±3.0 Ma for the Sangxiu volcanic rocks (Zhu et al., 2005) is essentially the same as the ~130 Ma that was proposed previously (Johnson et al., 1976; Veevers and McElhinny, 1976; Larson, 1977; Coffin et al., 2002; Ingle et al., 2002b) for the tectonic evolution of Eastern Gondwanaland. In this contribution, we present major, trace element and Sr–Nd isotopic data on representative samples of volcanic rocks from the Sangxiu Formation, and interpret these data in terms of their tectonic implications.

2. Geological setting and stratigraphy

The Tethyan Himalaya, which has been dominated by marine sedimentary sequences since the Paleozoic, is considered to have been a typical passive continental margin on the northern edge of Greater India from the Late Triassic to the Early Cretaceous (Yu and Wang, 1990). It is also interpreted as having developed in an extensional setting during continental breakup from the Middle-Late Paleozoic to the Early Cretaceous (Sciunnach and Garzanti, 1997; Garzanti et al., 1999; Wang et al., 2000). The Tethyan

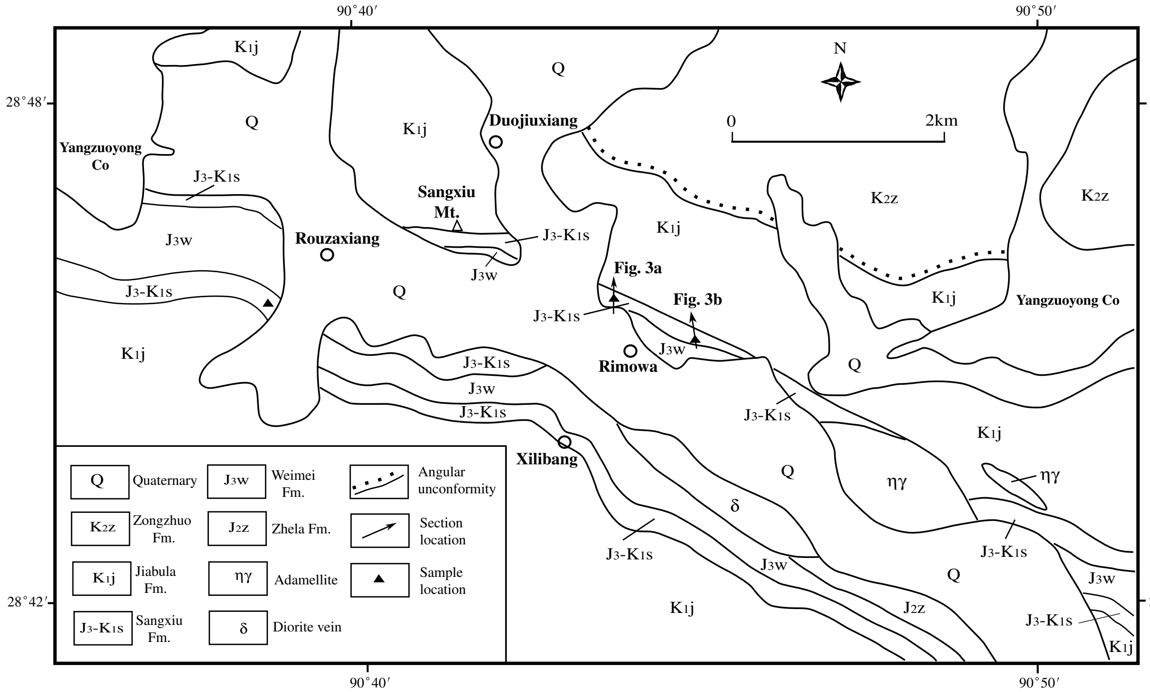

Fig. 2. Geological map of the studied area (Zhong et al., 2003, unpublished).

Himalaya is divided by the E–W Gyirong–Tingri–Ganba–Lhozhag fault over a distance of ~800 km, into two belts: the Northern Himalayan Belt in the south; and the Lhagoi Kangri Belt in the north. The Northern Himalaya Belt consist of shallow water carbonates and clastic rocks which were deposited throughout the Paleozoic (e.g. Pali area) and the Mesozoic–Cenozoic (e.g. Ganba Basin). The Lhagoi Kangri Belt can be further divided into two sub-belts on the basis of the style of deformation and their sedimentary sequences. The southern Lhagoi Kangri Sub-belt is composed of Precambrian Lhagoi Kangri metamorphic rocks, Ordovician marble and schist, Carboniferous marble, crystalline limestone and spotted slate, Permian slate and quartzite, Triassic flysch, and sporadic Jurassic and Cretaceous sequences. The northern Lhagoi Kangri Sub-belt consists mainly of Jurassic–Paleogene marine strata and some Triassic strata, showing only weak deformation and metamorphism. The Sangxiu Formation described in this account is located to the southeast of Yangzuoyong Co, in the northern Lhagoi Kangri Sub-belt (Fig. 1a).

The Sangxiu Formation is concordant to both the underlying Late Jurassic Weimei Formation and the overlying Early Cretaceous Jiabula Formation (Zhong et al., 2003). The Sangxiu volcanic rocks consist of basalts varying in thickness in different outcrops, with massive, amygdaloidal, pillow structures. Additionally felsic volcanic rocks are also observed in Rimowa and Zhegu Co (Fig. 1a). In Duojiuxiang (Figs. 2 and 3a), basalts of the Sangxiu Formation occur as massive flows and pillows of varying size. The rock assemblages of the Sangxiu Formation in Rimowa include (Figs. 2 and 3b): ≥ 6.5 m thick massive, amygdaloidal basalts at base, overlain by quartz sandstones, greywackes and siltstones (14.6 m) as well as shales, tuffs with intercalated pelitic siltstone and a minor thin-bedded quartz–sandstone lens (57.5 m). The latter is overlain by felsic volcanic rocks (130 m) and tuffs (35 m). Columnar jointing and a zone of weathering/alterations (2 m) are conspicuous in the felsic volcanic strata. Although, there are a series of clastic sediments overlying the basalts, as discussed by Zhu et al. (2005), basaltic magmatism occurred only slightly earlier than the eruption of the felsic volcanism. The thickness of the basalts in the middle-lower parts of the Sangxiu Formation range from several meters to 150 m (e.g. Xilibang), with an average thickness of ~100 m, and a volume of ~1000 km^3.

Petrographically, the Sangxiu volcanic rocks are extensively altered, however, original textures appear to have been preserved. In hand specimens, most Sangxiu basalts are largely aphyric, with the exception of sample SXI(2)-1 that contains microvesicles filled with chlorite and carbonate, while the felsic volcanic rocks are mostly phyric. In thin section, the Sangxiu basalts have a porphyritic texture (phenocrysts ~8–10%) dominated by anorthitic plagioclase phenocrysts (limited alteration), with a little highly altered clinopyroxene (e.g. carbonate and uralite). The groundmass consists chiefly of plagioclase with subordinate augite. Accessory minerals are ilmenite, titanite and variable amounts of magnetite, zircon and marcasite. Phenocrysts (10–12%) in the Sangxiu felsic volcanic rock are mainly potassic feldspar, plagioclase, quartz, biotite and hornblende. The feldspars are extensively altered (e.g. kaolinite, sericite). The quartz phenocrysts are corroded with embayed outlines. Carbonate minerals (e.g. siderite) and magnetite substitute for biotite, and chlorite replaces

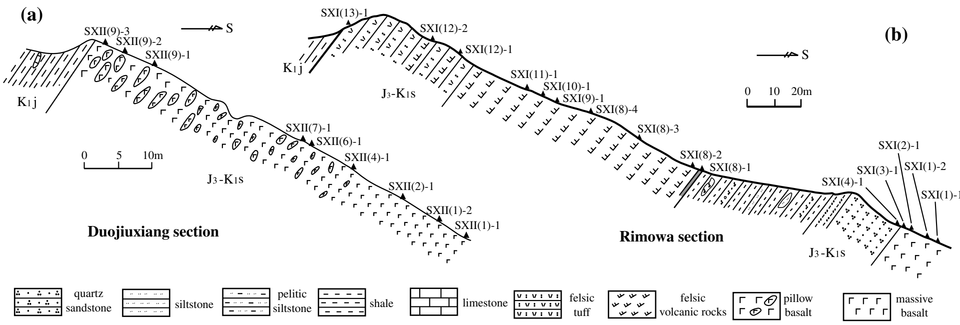

Fig. 3. Sections of the Sangxiu volcanic rocks in Duojiuxiang (a) and Rimowa (b).

hornblende. The groundmass consists of fine-grained feldspar, quartz, chlorite, sericite and volcanic ash. Accessory minerals include magnetite, ilmenite, zircon, limonite, and some unidentified species.

3. Analytical methods

Samples were collected from Rimowa, Duojiuxiang and Rouzaxiang (Fig. 2). Petrographically fresh samples were selected for geochemical analysis. Major element data were collected using X-ray fluorescence (XRF) in the Analytical Center, Chengdu Institute of Geology and Mineral Resources, the analytical uncertainties of XRF data are better than ~2% for Si, Ti, Al, Fe, Mg and Ca, and 3–5% for Mn, Na, K and P. Trace element data were determined using a Perkin Elmer Elan 6000 for acid dissolution inductively coupled plasma mass spectrometer (ICP-MS) at the Wuhan Analytical Center of Rocks and Minerals, Hubei. The analytical procedure used for ICP-MS analysis was similar to that described by Liu et al. (1996). Analytical uncertainties are generally less than 5% for the trace elements. Sr and Nd isotopic compositions of samples were measured by Finnigan MAT262 at the Institute of Geology and Geophysics, the Chinese Academy of Sciences, using the sample preparation procedure described by Cheng et al. (1987). The concentrations of Rb, Sr, Sm and Nd were analyzed by isotopic dilution. The measured $^{143}Nd/^{144}Nd$ and $^{87}Sr/^{86}Sr$ ratios were normalized to $^{146}Nd/^{144}Nd = 0.7219$ and $^{86}Sr/^{88}Sr = 0.1194$, respectively. The BCR-1 standard measured during the course of analyses gave an average $^{143}Nd/^{144}Nd$ of 0.512555±10 (2σ), NBS-987 gave $^{87}Sr/^{86}Sr = 0.704979 \pm 11$ (2σ). These analytical data are given in Tables 1 and 2.

4. Results

4.1. Alteration effects on major and trace elements

The Sangxiu volcanic rocks were altered to varying degrees after eruption, judging from petrographic observation and variable LOI in analyzed samples (2.04–9.57%). Hence, it is important to first estimate the effects of alteration on the analyzed samples before interpreting the analytical results. A general consensus exists that transition metals (e.g. Cr, Ni), rare-earth elements (REE), and high-field strength elements (HFSE) as well as Th and Ti in igneous rocks are relatively immobile during low-temperature alteration (e.g. Ludden and Thompson, 1978; Bienvenu et al., 1990; Staudigel et al., 1996). Indeed, as will be shown below, the REE and HFSE contents of our samples show subparallel concentration patterns. Thus, in general, the Sangxiu volcanic rocks analyzed still preserve some of their original trace element signature. However, some mobile elements such as Ba, K, Na, Rb, Sr, and to a certain extent U, show variable concentrations, implying that their original concentrations are likely to have been changed by alteration. Thus, only immobile elements such as the high-field strength elements (Ti, Zr, Y, Nb, Ta, Hf), Th and REE are used in the following discussion to identify the magmatic affinity and petrogenesis of these altered volcanic rocks.

4.2. Major-element geochemistry

The Sangxiu basic volcanic rocks have a relatively wide range of SiO_2 content and are of basalt to basaltic andesite composition (Table 1). Note that sample SXI (2)-1 has the lowest content of SiO_2 (44.54%) with the highest LOI value (9.56%), which can be ascribed to a high degree of alteration and to amygdaloidal structures filled with carbonate and chlorite. These basalts have high contents of TiO_2 (2.15–4.66%), comparable to the representative alkaline OIB ($TiO_2 = 2.87\%$, Sun and McDonough, 1989), while slightly lower than those of the Emeishan high-Ti basalts ($TiO_2 =$ 3.58–5.21%, Xiao et al., 2004). Also note that these basalts are characterized by remarkably low contents of MgO (1.11–6.23%) with Mg# range from 24.93 to 52.27, which are similar to those of the Emeishan high-Ti basalts (MgO = 2.26–6.88%, Xiao et al., 2004), suggesting a relative large degree of magmatic differentiation. The Sangxiu felsic volcanic rocks have a relatively small range of SiO_2 contents (62.68–72.10%) and are of dacite–rhyolite composition (Table 1).

On the Zr/TiO_2 vs. Nb/Y diagram of Winchester and Floyd (1977), the Sangxiu volcanic samples plot into the alkaline basalt field and the rhyolite–dacite field (Fig. 4). Note that a 'Daly gap' can be observed from the analyzed samples shown in Table 1 and Fig. 4, indicating that the Sangxiu volcanic rocks have an affinity with bimodal volcanic rocks.

Table 1
Major (wt%) and trace element (ppm) abundances of representative samples from the Sangxiu Formation in the central segment of Tethyan Himalayas

Sample#	RZ01-1	SXII(1)-1	SXII(1)-2	SXII(7)-1	SXII(9)-1	SXII(9)-3	SXI(1)-1	SXI(1)-2	SXI(2)-1	SXI(8)-3	SXI(8)-4	SXI(9)-1	SXI(10)-1	SXI(12)-2	SXI(13)-1
Location	1	2	3	4	5	6	7	8	9	10	11	12	13	14	15
SiO_2	50.4	49.82	49.32	56.58	47.72	48.2	52.58	53.16	44.54		67.74	67.16	71.84	72.1	62.68
TiO_2	3.77	2.52	4.15	4.45	4.66	4.09	2.15	2.16	3.23		0.52	0.77	0.61	0.63	0.58
Al_2O_3	12.7	13.01	12.76	13.92	13.63	13.12	14.04	13.79	15.16		13.97	14.6	12.57	12.56	17.09
Fe_2O_3	12.11	12.88	13.22	7.52	13.06	12.80	11.72	12.07	12.85		5.22	4.61	3.82	3.35	6.94
MnO	0.16	0.128	0.19	0.064	0.19	0.25	0.164	0.155	0.131		0.074	0.1	0.045	0.042	0.052
MgO	5.24	5.46	5.89	1.11	5.71	6.23	4.47	4.8	2.88		0.88	0.79	0.71	0.73	2.26
CaO	4.98	6.65	5.9	3.74	6.97	5.3	7.15	6.05	7.43		1.22	2.47	0.72	1.04	0.56
Na_2O	4.32	3.85	3.61	6.19	4.05	2.97	3.08	3.87	3.27		2.71	2.73	2.12	2.91	2.09
K_2O	0.21	0.73	1.18	0.12	0.35	0.091	0.08	0.26	0.75		4.56	3.97	4.69	3.88	3.75
P_2O_5	0.43	0.44	0.53	0.60	0.57	0.56	0.47	0.47	0.55		0.29	0.29	0.30	0.30	0.36
LOI	6.12	4.65	3.56	5.14	3.68	6.54	4.17	3.48	9.57		2.42	3.21	2.22	2.04	3.5
Total	99.77	99.29	99.48	99.30	99.63	99.23	99.30	99.41	99.38		99.32	100.44	99.37	99.35	99.37
$Mg^{\#}$	49.33	48.82	50.06	24.93	49.59	52.27	46.18	47.22	33.52		27.50	27.83	29.49	32.90	42.29
La	29.49	34.25	37.68	38.05	37.92	33.46	35.41	36.4	39.06	81.76	87.16	84	79.78	77.19	111.8
Ce	63.23	76.26	79.1	85.59	86.29	75.25	76.4	80.67	82.48	143	153.9	162	153.5	154.4	223.1
Pr	8.43	10.44	10.74	11.57	11.76	10.36	10.18	10.38	11.12	18.31	19.87	19.15	18.67	18.29	25.99
Nd	37.91	46.42	47.2	52.36	52.45	45.26	44.49	45.57	49.42	71.92	76.4	72.53	70.31	68.95	98.31
Sm	8.73	10.44	10.56	11.55	11.64	10.43	9.92	10.28	10.51	13.6	14.06	13.53	12.9	12.98	18.13
Eu	3.00	3.37	3.50	4.05	3.86	3.4	3.43	3.07	3.13	2.47	2.51	2.42	2.29	2.36	2.77
Gd	8.35	9.68	10	10.78	11.14	9.78	9.43	9.84	9.88	11.42	12.03	11.46	11.13	11.15	15.67
Tb	1.25	1.44	1.51	1.56	1.63	1.44	1.4	1.46	1.45	1.33	1.42	1.72	1.65	1.67	2.31
Dy	6.73	7.83	7.99	8.23	8.90	7.77	7.54	7.66	8.01	9.00	9.41	9.51	9.25	9.17	12.65
Ho	1.21	1.41	1.44	1.46	1.60	1.45	1.38	1.43	1.45	1.77	1.86	1.84	1.84	1.8	2.46
Er	2.98	3.51	3.55	3.49	3.96	3.48	3.44	3.47	3.57	4.76	4.99	4.97	4.83	4.82	6.5
Tm	0.43	0.5	0.52	0.5	0.56	0.51	0.51	0.5	0.5	0.71	0.74	0.79	0.76	0.75	1.03
Yb	2.46	2.85	2.87	2.69	3.14	2.85	2.85	2.98	3.01	4.24	4.54	4.82	4.83	4.75	6.32
Lu	0.35	0.4	0.41	0.38	0.44	0.41	0.4	0.43	0.42	0.64	0.68	0.72	0.73	0.71	0.98
Eu/Eu*	1.06	1.01	1.03	1.09	1.02	1.01	1.07	0.92	0.92	0.59	0.58	0.58	0.57	0.59	0.49
$(La/Yb)_N$	8.60	8.62	9.42	10.15	8.66	8.42	8.91	8.76	9.31	13.83	13.77	12.50	11.85	11.66	12.69
B	3.00	12.5	14	8.4	11.2	2.2	24.5	16	27.7	34	16.6	13.5	20.2	14.1	38.7
V	300	306	310	326	336	312	267	266	278	61	61	55	56	54	73
Cr	54.4	79.2	116.7	87.2	133.7	128.8	59.2	53.1	67.6	25	22	26.5	24.2	29.5	24.4
Sc	24.6	23.9	24.3	27.5	26.2	24.2	22.2	21.8	23.3	13.0	14.3	11.8	13.1	13.6	18.4
Ga	34.1	30	30	25.8	52	23.2	31.9	32.5	32.3	26.2	28.9	26.2	26.1	21.5	40.1
Rb	12.6	11	21.4	4.6	5.4	1.63	1.07	7.7	22.8	125.4	143.8	130.8	153.7	108.1	170
Sr	352	161	552	180	360	258	680	344	244	71	83	106	74	126	123
Y	28.63	33.23	33.66	32.97	37.26	33.55	33.16	32.92	33.84	43.52	44.81	45.15	43.57	43.34	57.95
Zr	292	356	368	362	397	347	342	336	368	512	521	493	472	468	643
Nb	30	37.6	38.7	37.4	41.6	36.8	31.6	31.6	34.9	26.1	25.7	26.7	24.7	24.3	32.8
Cs	13.7	7.3	7.3	7.3	6	3.2	4.7	3.2	2.1	3.2	2.8	2.1	2.8	2.4	3.4
Ba	409	418	710	155	1696	270	168	234	434	840	1110	857	1101	1237	1254
Hf	6.4	7.3	7.9	10.5	8.6	7.8	7.1	7.3	8.3	12.4	13.3	12.1	12.2	12.6	17.6
U	1.47	1.88	1.28	1.09	1.54	1.39	1.23	1.31	1.13	2.32	0.64	2.49	2.47	2.27	2.73
Th	3.0	3.1	3.1	4.0	3.0	3.0	4.1	3.6	3.5	29.4	28.9	27.6	34.5	37.1	48.5
Ta	2.6	3.5	3.2	3.3	3.1	3.1	2.2	3.2	1.7	1.3	1.8	2.2	2.6	1.2	2.8

Sampled locations: 1. sampled from Rouzaxiang; 2–6. sampled from Duojiuxiang; 7–15. sampled from Rimowa. Rock types: 1–9. basalts; 10–14. felsic lavas; 15. felsic tuff (data from Zhu et al., 2005); Mg# = 100×Molar $Mg^{2+}/(Mg^{2+}+Fe^{2+})$], assumed $Fe^{3+}/Fe^{2+}=0.15$. Total iron as Fe_2O_3. Eu/Eu* = $2*Eu_N/(Sm_N+Gd_N)$, the subscript of N means normalized to chondrite (Sun and McDonough, 1989).

Table 2
Rb–Sr and Sm–Nd isotopic data of representative samples from the Sangxiu Formation in the central segment of Tethyan Himalayas

Sample	Rb (ppm)	Sr (ppm)	$^{87}Rb/^{86}Sr$	$^{87}Sr/^{86}Sr \pm 2\sigma m$	$(^{87}Sr/^{86}Sr)_t$
SXI(12)-2	110.7	126.9	2.53	0.726431±14	0.721648
SXI(9)-1	128.9	129.7	2.883	0.729021±13	0.723571
SXI(8)-3	121.9	73.78	4.793	0.731036±13	0.721975
SXI(1)-2	8.49	387.6	0.0634	0.710024±25	0.709904
SXI(1)-1	1.07	753.4	0.0041	0.709135±7	0.709127
SXII(1)-1	11.1	196.1	0.1639	0.707680±13	0.707370
SXII(9)-3	1.63	273.7	0.0173	0.707788±17	0.707755

Sample	Sm (ppm)	Nd (ppm)	$^{147}Sm/^{144}Nd$	$^{143}Nd/^{144}Nd \pm 2\sigma m$	$(^{143}Nd/^{144}Nd)_t$	$\epsilon Nd(t)$	T_{DM} (Ma)
SXI(12)-2	12.71	68.15	0.1128	0.511896±9	0.511798	−13.05	1892
SXI(9)-1	13.25	70.27	0.1140	0.511880±7	0.511781	−13.39	1939
SXI(8)-3	13.64	72.77	0.1134	0.511892±7	0.511793	−13.14	1909
SXI(2)-1	10.01	45.97	0.1317	0.512552±12	0.512437	−0.57	
SXI(1)-2	9.46	42.36	0.1351	0.512587±6	0.512469	0.05	
SXI(1)-1-(2)	9.81	43.8	0.1354	0.512556±12	0.512438	−0.56	
SXI(1)-1	9.28	41.42	0.1355	0.512497±11	0.512379	−1.71	
Pyroxene in SXI(1)-2	9.96	44.17	0.1363	0.512527±8	0.512408	−1.14	
SXII(1)-1	10.27	45.45	0.1366	0.512688±7	0.512569	2.00	
SXII(9)-3	9.94	42.64	0.141	0.512619±10	0.512496	0.58	

m, measured isotopic ratios; *t*, age-corrected initial isotopic ratios (133 Ma for age correct after Zhu et al., 2005). $\varepsilon Nd(t)$ are initial values; $\varepsilon Nd(t)$ values were calculated using present day $(^{143}Nd/^{144}Nd)_{CHUR} = 0.512638$ and $(^{147}Sm/^{144}Sm)_{CHUR} = 0.1967$ (CHUR = chondritic uniform reservoir; $\lambda = 6.54\times10^{-12}$ a^{-1}), $f_{Sm/Nd} = (^{147}Sm/^{144}Sm)_{sample}/(^{147}Sm/^{144}Sm)_{CHUR} - 1$; $f_{Rb/Sr} = (^{87}Sr/^{86}Sr)_{sample}/(^{87}Sr/^{86}Sr)_{U.R} - 1$ (U.R = earth uniform reservoir). The age of 133 Ma is used for $\varepsilon Nd(t)$ and $(^{87}Sr/^{86}Sr)_t$ calculations; $[(^{87}Sr/^{86}Sr)_t = (^{87}Sr/^{86}Sr)_m - ^{87}Rb/^{86}Sr\ (e^{IËt} - 1)$; $\lambda = 1.42\times10^{-11}$ a^{-1}]; T_{DM} is the Nd isotopic model age related to depleted mantle, T_{DM} represents the age of crustal material separated from depleted mantle. Nd isotopic data after from Zhu et al. (2005) except for the samples SXII(1)-1, SXII(9)-3.

4.3. Trace-element geochemistry

The Sangxiu basalts are notably fractionated between light rare earth element (REEs) and heavy REEs [$(La/Yb)_N = 8.42$–10.15, averaging 8.98], but lack a negative Eu anomaly (Eu/Eu* = 0.92–1.09), inconsistent with petrographic observations, will be discussed below. The low concentrations of HREE (Yb = 2.46–3.14 ppm), compatible elements (Cr = 54.4–133.7 ppm), which resemble to those of the Emeishan high-Ti basalts (Yb = 2.22–4.0 ppm, Cr = 20–106 ppm, Xiao et al., 2004) at the same MgO levels, suggesting light REE enriched sources with advanced degrees of fractional crystallization. The Sangxiu basalts are enriched in high field-strength elements (HFSEs; e.g. Nb = 30.0–41.6 ppm) that are lie within the Nb abundance range of the Emeishan high-Ti basalts (Nb = 25–68 ppm, Xiao et al., 2004).

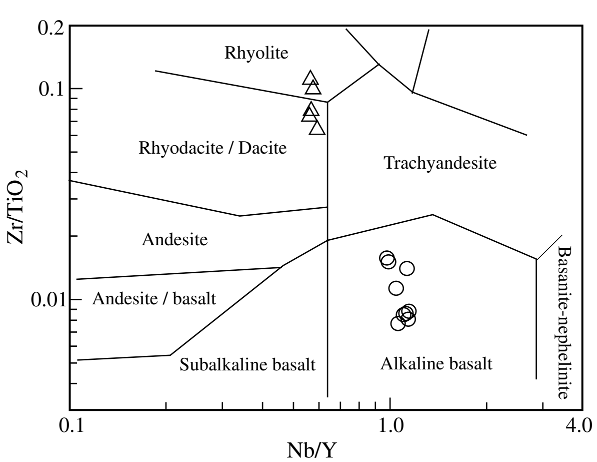

Fig. 4. Nb/Y–Zr/TiO_2 diagram of Winchester and Floyd (1977) showing the alkaline basalt (circles), rhyolite–dacite (triangles) affinity of the Sangxiu volcanic rocks.

All but one (RZ01-1) basaltic sample have relatively uniform REE in the chondrite-normalized REE patterns (Fig. 5a). Although sample RZ01-1 has the lowest LREE ($La_N = 124$) and REE absolute abundance, showing a subparallel REE pattern with the other samples. In the primitive mantle-normalized spidergrams (Fig. 6a, Sun and McDonough, 1989), all the basaltic samples have 'humped', subparallel patterns, characterized by variable enrichment in all the trace elements with respect to the primitive mantle. Nb and Ta show slightly negative to positive anomalies relative to the neighboring elements (e.g. Nb/La = 0.87–1.10), resembling many alkali basalts formed in continental rifts or oceanic islands, with little or no appreciable crustal contamination. Sample RZ01-1 lacks a Nb–Ta anomaly (Nb/La = 1.02). Note that all the basalts are depleted in P, indicating a crystallization of apatite.

Samples were normalized to chondrite, primitive mantle composition to test the nature of the magma source region. The chondrite-normalized REE patterns (Fig. 5a) and trace element spidergrams (Fig. 6a) of the Sangxiu basalts are broadly similar to those of the Emeishan high-Ti basalts, which may suggest a similar petrogenesis. These basalts exhibit slight differences from representative alkaline OIB (e.g. relatively higher HREE), which may indicate the compositional differences in the magma source region. In addition, the Sangxiu basalts share most of the geochemical features of the Rajmahal alkaline basalts, and plot within

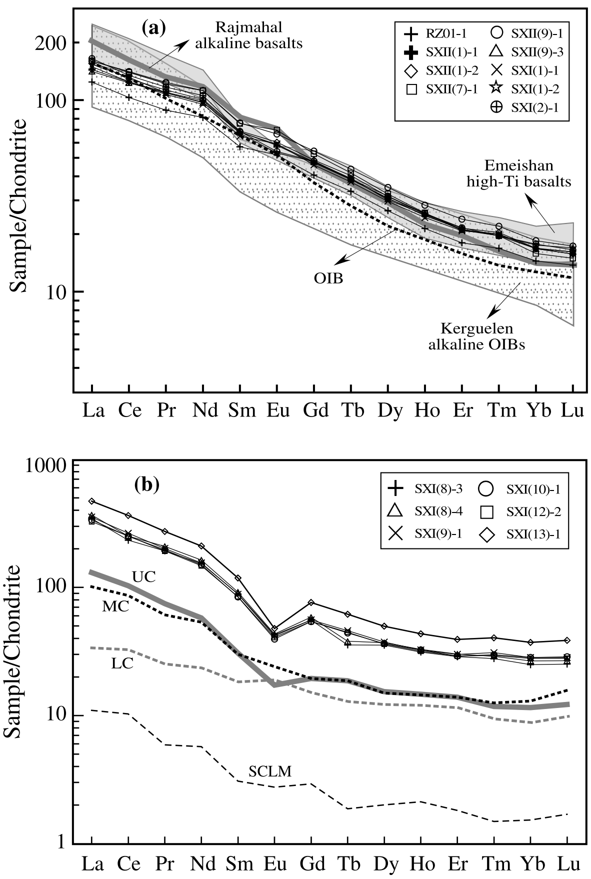

Fig. 5. (a,b) Chondrite-normalized REE diagrams for Sangxiu volcanic rocks. Normalizing values and OIB data are from Sun and McDonough (1989); the Emeishan high-Ti basalts are from Xiao et al. (2004); subcontinental lithospheric mantle (SCLM) values are from McDonough (1990); upper crust (UC), middle crust (MC) and lower crust (LC) values are from Rudnick and Gao (2003); Rajmahal alkaline basalts, Kerguelen alkaline basalts are from http://georoc.mpch-mainz.gwdg.de/georoc/Entry.html.

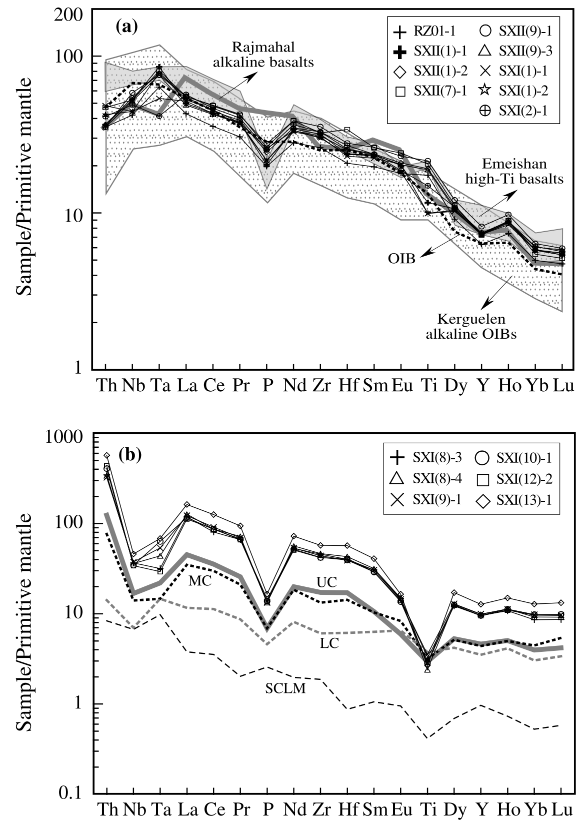

Fig. 6. (a,b) Primitive mantle-normalized trace element diagrams for the Sangxiu volcanic rocks. Normalizing values and plotting order are from Sun and McDonough (1989). Data source are same as the Fig. 5.

the field of the Kerguelen alkaline basalts (Figs. 5a and 6a), which seems to imply a similar mantle plume-related magma source region.

The Sangxiu felsic volcanic lavas have high Zr (468–521 ppm), Nb (24.3–32.8 ppm) and Hf (12.1–17.6 ppm) with a moderate negative Eu anomaly (Eu/Eu* = 0.57–0.59). The chondrite-normalized REE diagram (Fig. 5b) show coherent, subparallel REE patterns with significant enrichment in LREE relative to HREE. Chondrite-normalized $(La/Yb)_N$ ratios for these felsic lavas are between 11.66 and 13.83. Note that the felsic tuff (sample SXI(13)-1) has subparallel pattern with the felsic lavas, although it has higher absolute abundances. In the primitive mantle-normalized spidergrams (Fig. 6b; Sun and McDonough, 1989), the Sangxiu felsic volcanic rocks display an overall enriched pattern, except for depletion in Nb, Ta, P, Eu and Ti due to fractional crystallization. The chondrite-normalized REE patterns (Fig. 5b) and trace element spidergrams (Fig. 6b) of the analyzed felsic samples are subparallel to those of the middle and upper crust (Figs. 5b and 6b) although they have higher absolute abundances, which may suggest a petrogenetic relationship with the middle and upper crust.

4.4. Sr–Nd isotopes

Measured and age-corrected isotopic data are given in Table 2. Measured isotopic ratios of the Sangxiu basalts vary in $^{87}Sr/^{86}Sr$ ratios from 0.70768 to 0.710024 and $^{143}Nd/^{144}Nd$ ratios from 0.512497 to 0.512688. Initial isotopic ratios were calculated for an age of 133 Ma (Zhu et al., 2005). Initial strontium ratios $(^{87}Sr/^{86}Sr)_{133\ Ma}$ range from 0.70737 to 0.709904 and initial neodymium isotopic ratios $(^{143}Nd/^{144}Nd)_{133\ Ma}$ from 0.512379 to 0.512569 ($\varepsilon Nd(t)_{133\ Ma} = -1.71$ to 2.00), similar to those of the Emeishan high-Ti basalts ($\varepsilon Nd(t) = -1.17$ to 0.43, Xiao et al., 2004).

The Sangxiu felsic volcanic rocks have a restricted range of $^{143}Nd/^{144}Nd$ (0.51188–0.511896) that differs significantly from the values of basalts. Initial $(^{143}Nd/^{144}Nd)_{133\ Ma}$ range from 0.511781 to 0.511798 ($\varepsilon Nd(t)_{133\ Ma} = -13.39$ to -13.05). The $^{87}Sr/^{86}Sr$ of felsic volcanic rocks ranges from 0.726431 to 0.731036, with corresponding initial $(^{87}Sr/^{86}Sr)_{133\ Ma}$ values of 0.721648–0.723571. In general, the Sangxiu felsic volcanic rocks have much higher radiogenic Sr isotopic and unenriched Nd isotopic compositions than those of the Sangxiu basalts.

5. Discussion

5.1. Tectonic setting

Meschede (1986) showed that within-plate alkaline basalt and E-MORB could be identified without ambiguity on the triangular plot of Zr–Nb–Y, which is also confirmed by Rollinson (1993). Additionally, Yb is assumed to be immobile, and to behave as an incompatible element, so the ratio of two incompatible elements such as Th/Yb will remain unchanged during partial melting and fractional crystallization. The same will be true for the Ta/Yb ratio, and variations on a Th/Yb vs. Ta/Yb diagram therefore reflect differences in source composition (Pearce, 1983; Rollinson, 1993). The Zr–Nb–Y and Th/Yb–Ta/Yb diagrams (Fig. 7a,b) illustrate that the Sangxiu basalts are characteristic of within-plate alkaline basalts, which to a large extent resemble the representative OIB (Sun and McDonough, 1989) and the Emeishan high-Ti basalts (Xiao et al., 2004).

Condie (1986) showed that the felsic volcanic rocks formed in an extensional setting have higher Zr and Hf concentrations (> 200, > 6 ppm, respectively) than those of the felsic rocks formed in an island arc setting. It is most likely that the Sangxiu felsic volcanic rocks are related to an extensional setting due to their high abundances of Zr (468–643 ppm)m and Hf (12.1–17.6 ppm). This setting is also supported by immobile element discrimination diagrams (e.g. Nb vs. Y). Y and Nb were selected as two of the most efficient discriminants between most types of ocean-ridge granite, within-plate granite, volcanic-arc granite and syn-collisional granite (Pearce et al., 1984; Rollinson, 1993). In this diagram, the Sangxiu felsic volcanic rocks plot in the 'within-plate' setting field (Fig. 7c).

The underlying Late Jurassic Weimei Formation is composed chiefly of coarse quartz sandstone and intercalated mudstone with a high quartz content, shallow water ripple marks and relic fossils, which is considered to be a sedimentary record of a shore to shallow sea paleo-environment (Jiang et al., 2003). These rocks were followed by Sangxiu volcanism. The volcanic rocks are overlain by the Early Cretaceous Jiabula Formation composed of clastic rocks and calcic and silicic flysch, with the characteristics of deep-water sedimentation. A rapidly deepened upward rift succession is documented clearly from the underlying Weimei to the overlying Jiabula Formation. A two-layer stratigraphic structure including OIBs at base with the overlying pelagic sediments (carbonates and siliceous rocks) represents a typical ocean island environment. However, as far as the origin of the Sangxiu Formation is concerned, the volcanics are not overlain by pelagic sediments (carbonates and siliceous rocks) (Zhong et al., 2003). Taking the geochemical discrimination diagrams into account it is concluded that the Sangxiu basalts were not formed in an oceanic island setting, but in a continental rift setting, although the volcanic rocks have similar geochemical features to OIB.

Generally, basaltic lavas in a continental rift setting is associated with a mantle plume, the asthenosphere, the

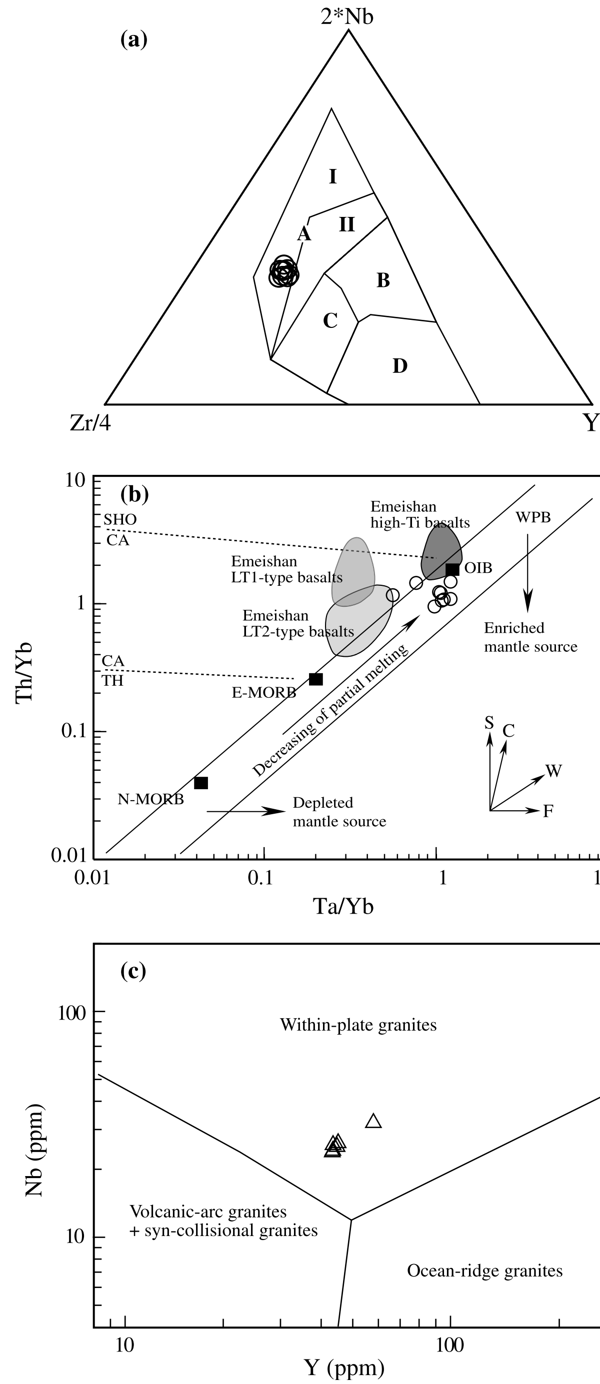

Fig. 7. (a) Nb–Zr–Y discrimination diagram (Meschede, 1986) for the Sangxiu basalts. The fields are defined as follows: AI, within-plate alkali basalts; AII, within-plate alkali basalts and within-plate tholeiites; B, E-type MORB; C, within-plate tholeiites and volcanic-arc basalts; D, N-type MORB and volcanic-arc basalts. (b) Th/Yb–Ta/Yb discrimination diagram (Pearce, 1983) for the Sangxiu basalts. Vectors indicate the influence of subduction components (S), within-plate enrichment (W), crustal contamination (C), and fractional crystallization (F). Note that the Sangxiu basalts plot close to representative OIB and toward the Emeishan high-Ti basalts. N-MORB, E-MORB and representative OIB values after Sun and McDonough (1989); the Emeishan LT1-, LT2-type, and high-Ti basalts are from Xiao et al. (2004). (c) Nb–Y discrimination diagram (Pearce et al., 1984) for the Sangxiu felsic volcanic rocks. Sample symbols as in Fig. 4. Note that the felsic rocks plot within the field of within-plate granites.

lithospheric mantle and continental crust (Sun and McDonough, 1989; Xu, 1999). Therefore, key to study the petrogenesis of mafic rocks is to identify the relative contributions made by mantle plumes, the normal asthenosphere, the lithospheric mantle and the continental crust.

5.2. Crustal contamination

Although enriched signatures of mafic lava in a continental rift setting could be attributed to contamination by continental crust, this contribution seems to have been very small in most of the Sangxiu basalts for the following reasons: 1). No clear mixing trend exists between the analyzed sample suites and average continental crust seen on discrimination diagrams such as Nb/Th vs. Ce (Fig. 8a), which would otherwise be expected (Tomlinson et al., 1999; Condie et al., 2002); and 2). On the $(Th/Ta)_{PM}$ vs. $(La/Nb)_{PM}$ diagram, the plots are close to the primitive mantle value, and obviously far from the average values of middle and upper continental crust (Fig. 8b); and 3. No crustal contamination trend is seen on the εNd(t) vs. 100/Nd diagram (Fig. 8c). It may be noted that samples SXI(1)-1 and SXI(1)-2 display a weak negative Nb anomaly (Nb/La = 0.87–0.89), suggesting a slight contamination from sub-continental lithospheric mantle and/or the lower crust (discussed below).

5.3. Fractionation crystallization vs. partial melting

As shown in Table 1, the Sangxiu basalts have a low MgO content with a low Mg number (Mg#) ranging from 24.93 to 52.27, suggesting an evolved compositional feature. In MgO vs. SiO_2 diagram (Fig. 9a), most Sangxiu basalt samples show a decrease in MgO with increasing SiO_2, indicating significant fractional crystallization of olivine and clinopyroxene. Most Sangxiu basalts show a positive correlation when Cr is plotted against MgO (Fig. 9b), the rapid decrease in Cr from 6.23 to 4.47% MgO can be ascribed to the fractionation of olivine with Cr-spinel. Decreasing TiO_2 with decreasing MgO indicates magnetite–titanomagnetite and/or ilmenite fractionation, accompanying olivine–clinopyroxene fractionation (Fig. 9c). Most Sangxiu basalts have relatively restricted Al_2O_3/CaO ratios, with the exception of sample SXII(7)-1. A constant Al_2O_3/CaO ratio with increasing SiO_2 (Fig. 9d) indicates that plagioclase fractionation was important. However, this is inconsistent with the absence of a negative Eu anomaly (Eu/Eu* = 0.92–1.09), and the negative correlation between Al_2O_3 and Mg# (Fig. 9e). Generally, with cooling and crystallization of a magma, Mg# decreases because of the separation of a mafic mineral (olivine, cpx, etc.) accompanied by plagioclase crystallization. However, if plagioclase separation from the residual melts is inefficient, abundant plagioclase phenocrysts (accumulation) would be left as a residual mineral in the samples. Therefore, more plagioclase in the rock gives higher Al_2O_3 while the bulk rock has a lower Mg#, that is, the

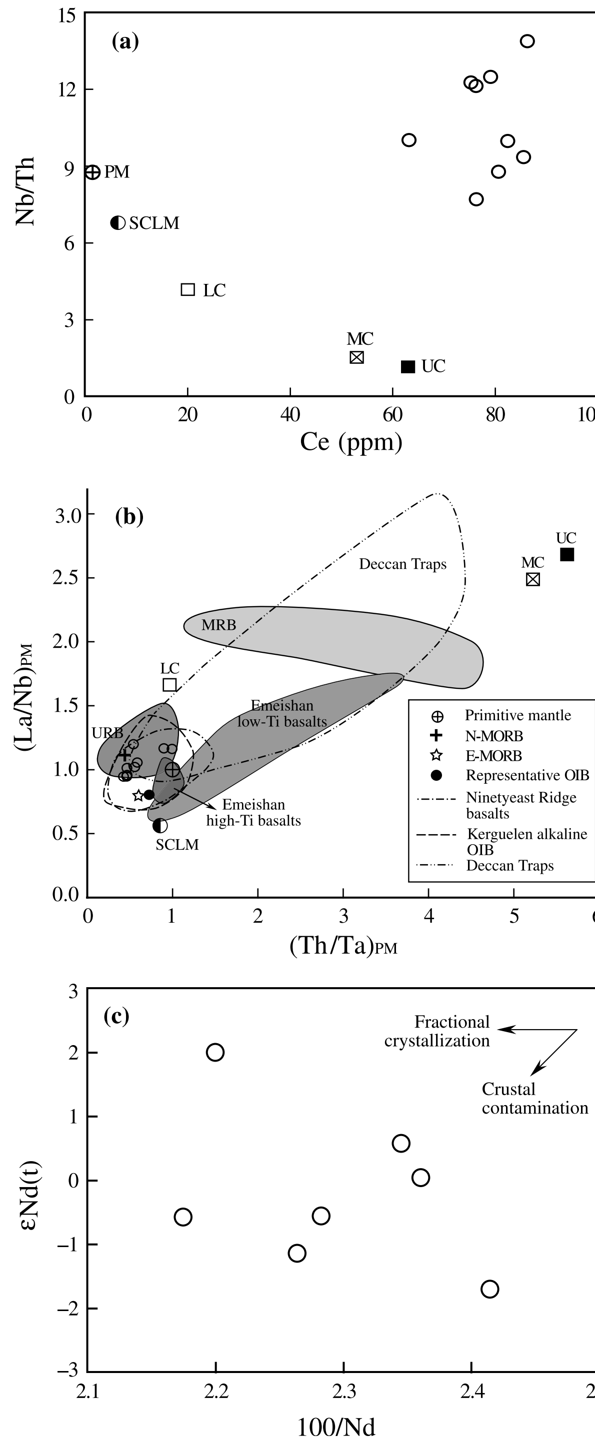

Fig. 8. (a,b,c) Discrimination diagrams for testing crustal contamination for the Sangxiu basalts. Data sources: primitive mantle (PM) values are from Sun and McDonough (1989), Emeishan low-Ti basalts are from Xiao et al. (2004); modified Rajmahal basalts (MRB), unmodified Rajmahal basalts (URB), Ninetyeast Ridge basalts, and Deccan Traps values are from http://georoc.mpch-mainz.gwdg.de/georoc/Entry.html; the others are same as Fig. 5. Sample symbols as in Fig. 4. Note that there is unappreciable crustal contamination for the most Sangxiu basalts.

negative trend observed in Fig. 9e and the absence of a negative Eu anomaly may very well result from plagioclase phenocryst accumulation, corresponding to the petrographic observations.

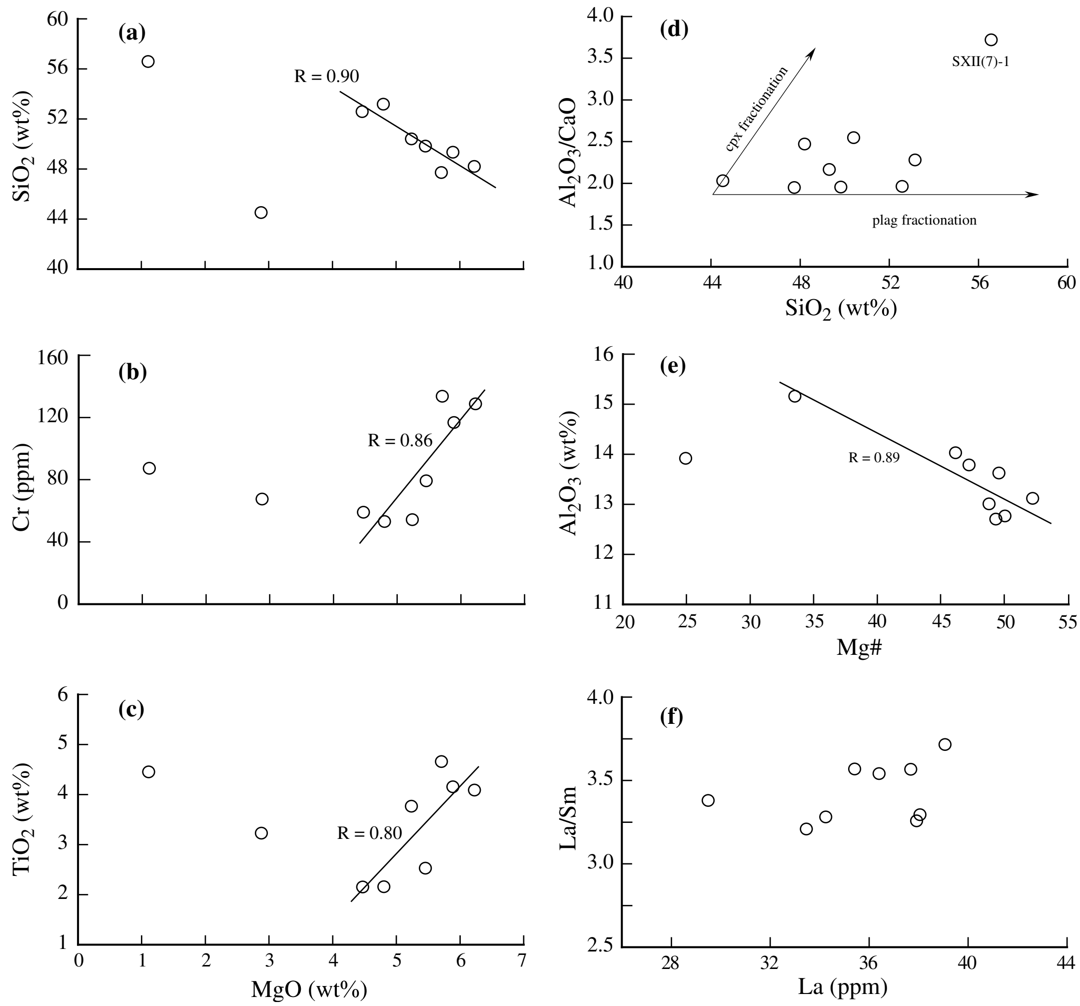

Fig. 9. Selected chemical variation diagrams to illustrate fractionation crystallization of the Sangxiu basalts.

Allegre and Minster (1978) showed that the ratio of the concentration of a highly incompatible element to a moderately incompatible element can be used to identify partial melting trends. In Fig. 10, data from the Sangxiu volcanic rocks have been plotted in $C^{Th}/C^{element}$ vs. C^{Th} diagrams, where C is the concentration of the element. In all the left diagrams (Fig. 10a–g), the Sangxiu basalts exhibit relatively well-defined linear trends, indicating that the basaltic magmas were generated by partial melting of mantle source materials. However, the La/Sm vs. La plots (Fig. 9f) of the analyzed basalt samples are scattered, failing to indicate either partial melting or fractional crystallization trends. This seems to suggest that the observed lava compositional variations in major elements and trace elements were inherited from fertile mantle sources. It should be noted that a partial melting trend can be observed within the analyzed felsic volcanic rock samples, with the exception of tuff sample SXI(13)-1(Fig. 10h–n).

5.4. Petrogenesis of basalts

The foregoing description suggests that the Sangxiu basalts may have been derived from mantle source materials resembling those of many oceanic island basalts. This will be further corroborated in the following discussion. Nb, Th and La are immobile elements, so that seawater alteration would not change the Nb/Th and La/Nb ratios. These ratios are also not susceptible to magma processes because they have similar partition coefficients. Li (1993) showed that the island arc basalts, MORB and OIB can be distinguished well by Nb/Th–Nb and La/Nb–La diagrams (Fig. 11). Obviously, the Sangxiu basalts all plot within the OIB field in these diagrams (Fig. 11a,b). In addition, although plots of the Sangxiu basalts are relatively discrete on the $(^{143}Nd/^{144}Nd)_{133\ Ma}$ vs. $(^{87}Sr/^{86}Sr)_{133\ Ma}$ diagram (Fig. 12a), they mostly plot within the field of Rajmahal basalts, interpreted to be the result of early activity of the Kerguelen hotspot (Kent et al., 2002).

On the other hand, a lithospheric mantle source seems also to be required for the Sangxiu basalts, although OIB-type characteristics exert a strong control on the trace element systematics of the these basalts.

There are three factors which may be responsible for the high initial Sr isotopic ratios of samples SXII(1)-1 and SXII(9)-3, which exhibit features of insignificant crustal contamination (such as Nb/La > 1, positive εNd(t) values):

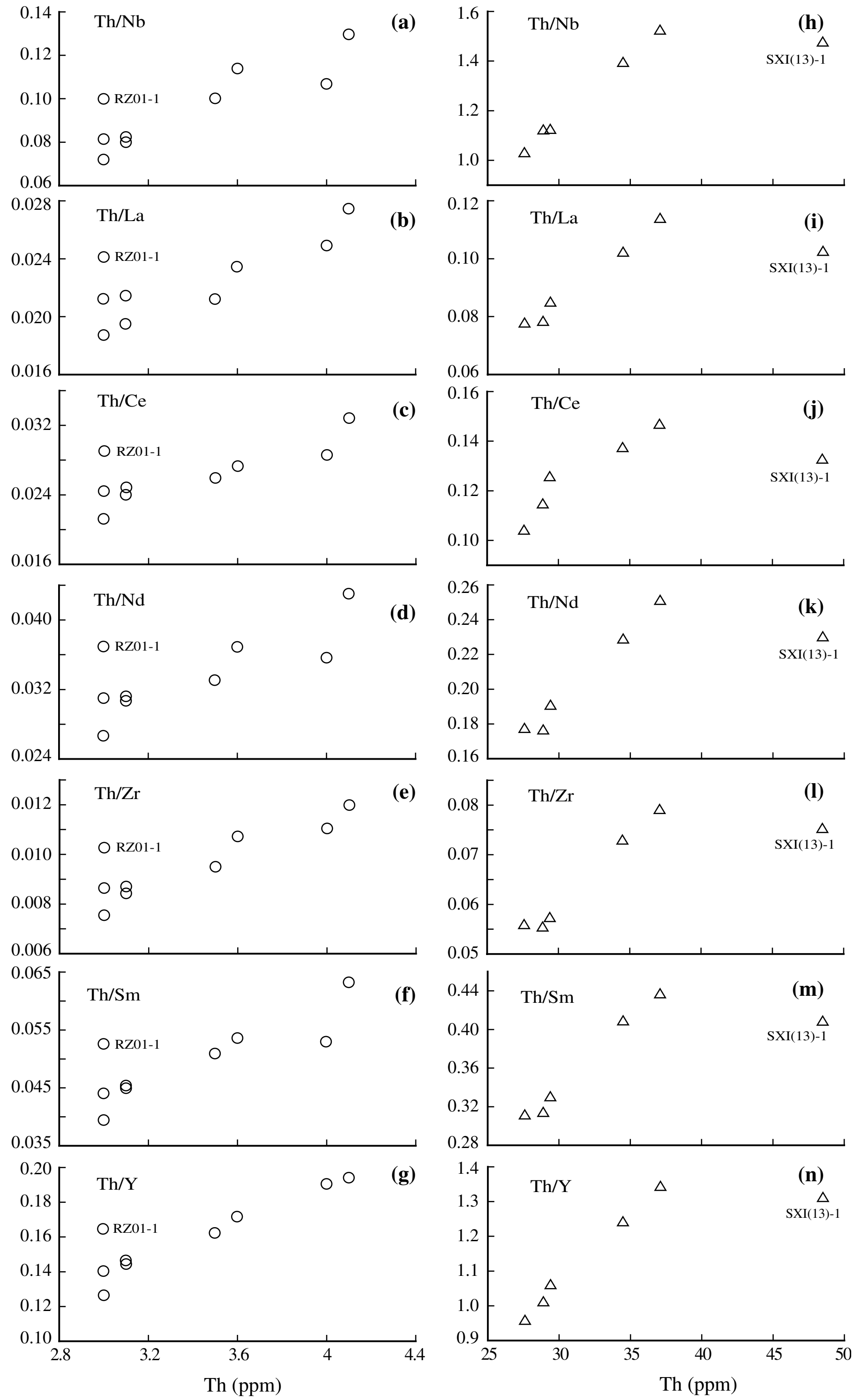

Fig. 10. TH/X vs. Th diagrams, where element X is Nb, La, Ce, Nd, Zr, Sm and Y. The linear correlations for the most Sangxiu basalts (left column, a–g) and the felsic rocks (right column, h–n) samples showing a trend of partial melting.

1). Alteration by seawater, which, with high Sr concentration (~8 ppm, Li, 1991) and high $^{87}Sr/^{86}Sr$ (today~0.709), would raise $^{87}Sr/^{86}Sr$ ratios in basalts (Mahoney et al., 1998), while seawater would not affect the Nd and Nd isotopes; 2). Kamenetsky et al. (2000) showed, using the case of Macquarie island alkali basalts, that a small but significant increase in $^{87}Sr/^{86}Sr$ ratio takes place with a decreasing degree of partial melt, while the $^{143}Nd/^{144}Nd$ ratio decreases. This is well documented in the Sangxiu basalts with a negative correlation between the Sr and Nd isotopic ratios (Fig. 12a). As shallow level cooling and fractionation cannot change $^{87}Sr/^{86}Sr$ ratio significantly without evidence for obvious crustal contamination, this correlation reflects primarily isotopic heterogeneity in the fertile mantle source

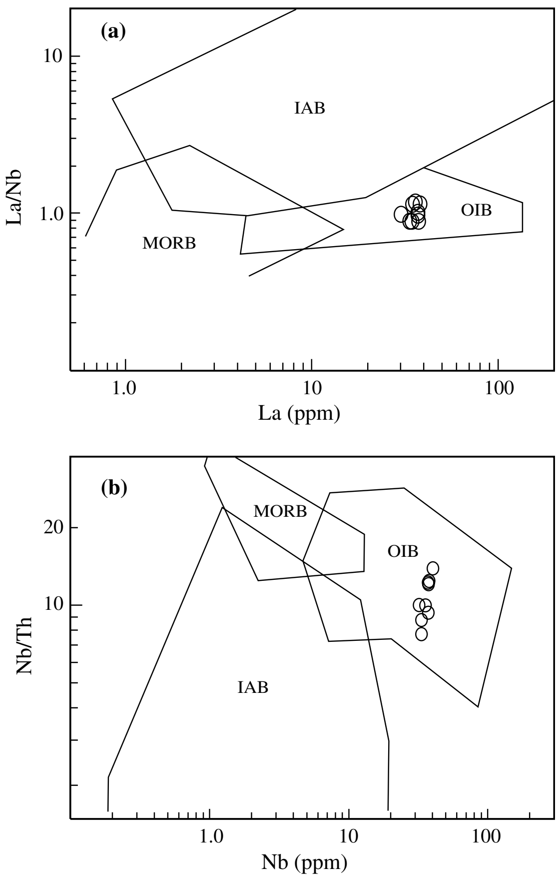

Fig. 11. Trace element discrimination diagrams (Li, 1993) for the Sangxiu basalts showing characteristics of an OIB-type source. The fields are defined as follows: IAB, Island-arc basalts; MORB, mid-ocean ridge basalts; OIB, oceanic island basalts.

(e.g. lithosphere) otherwise, melting will not fractionate the radiogenic isotope (Niu et al., 2002); and 3). Xu (1999) showed that the $^{87}Sr/^{86}Sr$ ratios of melts originated from mantle plumes are intermediate (0.7028–0.707) between those sourced from asthenospheric (0.7022–0.7028) and lithospheric mantle (0.7035–0.71), thus, the Sr isotopic ratios of mantle plume-derived melts will be increased when lithospheric materials are involved.

The Ce/Y–Zr/Nb diagram (Deniel, 1998) illustrates the approximate melt compositions of the Sangxiu basalts (Fig. 12b), which fall between the depleted garnet lherzolite (GD) and primitive garnet lherzolite (GP) non-modal fractional melting curves (much closer to the latter), suggesting that the magmas were formed by the melting of garnet lherzolite. The notable fractionation between the LREE and HREE ($(La/Yb)_N = 8.42–10.15$) and the high Ce/Yb ratios (25.70–31.82) of the Sangxiu basalts correspond a low degree of partial melting of garnet lherzolite (Lin and Stern, 1989), which is located in the lower part of lithosphere.

Trace element ratios such as Nb/Th and Ti/Yb are helpful in distinguishing crustal contamination from interaction with sub-continental lithospheric mantle, because these ratios are very sensitive to the crustal contamination of mantle-derived magmas (Li et al., 2002). In the Ti/Yb vs. Nb/Th plot (Fig. 13), most Sangxiu basalts show relatively uniform Ti/Yb and Nb/Th ratios, close to those of the representative alkaline OIB (Sun and McDonough, 1989). The lesser-contaminated basalts (samples SXI(1)-1, SXI(1)-2) plot apart from the trend of the addition of sialic crustal materials, but toward the sub-continental lithospheric mantle and/or the lower crust, with Ti/Yb and Nb/Th ratios intermediate between those of Hawaiian OIB and sub-continental lithospheric mantle. It is well known that there is no sub-continental lithospheric mantle beneath Hawaii, thus the Ti/Yb vs. Nb/Th plots seem imply that sub-continental lithospheric mantle and/or lower crust components were variably involved in the generation of the Sangxiu basalts.

In summary, major and trace element data, and Sr–Nd isotopic compositions, suggest that the Sangxiu basalts may have been derived from an OIB-type mantle source with a discernable contribution from subcontinental lithospheric mantle. With consideration of the broadly geochemical similarities between the Sangxiu basalts and the Emeishan high-Ti basalts, a model of plume–lithosphere interaction is attractive for the generation of the Sangxiu basalts. The Sangxiu basaltic magmas may have formed as a result of infiltration of plume-derived melts into the base of the lithosphere in a continental rift setting. The Sangxiu volcanism on northeastern margin of Greater India may represent an example of the interaction between a plume or hotspot and the lithosphere.

5.5. Petrogenesis of felsic rocks

The Sangxiu felsic volcanic rocks are high in LREE, Nb, Zr, Hf and Y, have relatively high Ga/Al ratios (3.23–4.43) and low P and Ti. Overall, they share most of the geochemical features of A-type granites (Whalen et al., 1987). For instance, in Ga/Al vs. Zr and Ga/Al vs. Nb plots they all fall into the A-type granite field and close to the typical A-type granite (Fig. 14a-b, Whalen et al., 1987).

Although there is growing evidence that some A-type magmas are differentiation products of mantle-derived melts through extensive fractional crystallization (Turner et al., 1992; Bonin, 1996), the petrogenesis of A-type magmas within a continental rift setting is still an issue of debate. The presence of a 'Daly gap' between mafic and felsic rocks and Nd isotopes appear to argue against a magma differentiation model. There are two mechanisms which could be considered for the petrogenesis of the Sangxiu felsic magmas: 1). Extensive fractional crystallization of mafic magmas, coupled with significant assimilation of continental crust (AFC processes) (Grove and Donnelly-Nolan, 1986; Bacon and Druitt, 1988; Ingle et al., 2002a), of which the εNd(t) values of the products are similar to those of the associated mafic rocks; and 2). Melting of ensialic continental crust (anatexis) in an intraplate environment (Cox, 1972; Bullen and Clynne, 1990; Roberts and Clemens, 1993; Tepper et al., 1993; Guffanti et al., 1996), showing enrichment in Al, Th, LREE and negative εNd(t) values distinctly differing from the associated mafic rocks.

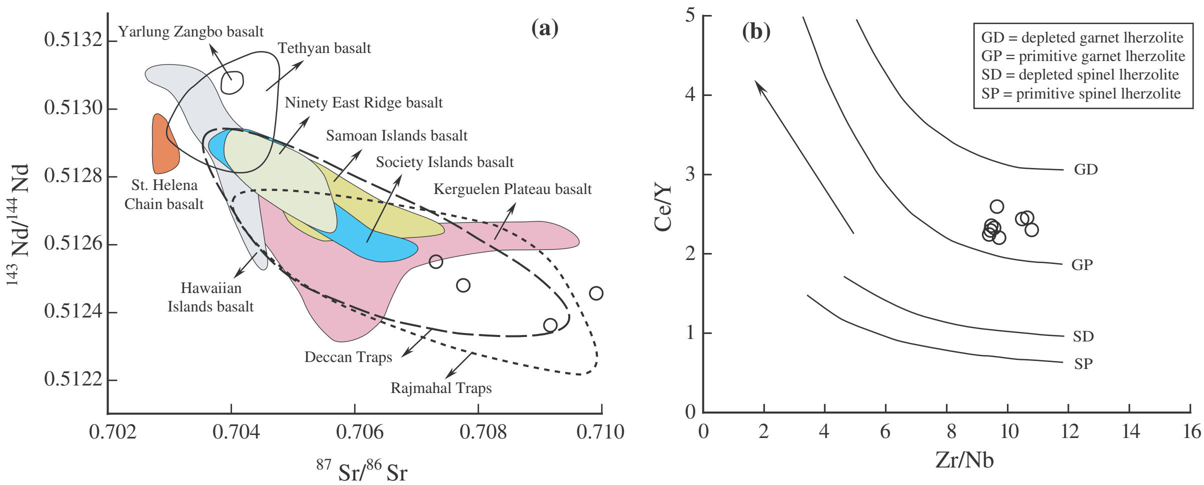

Fig. 12. (a) Sr–Nd isotopic diagram for the Sangxiu basalts. Tethys, Yarlung Zangbo basalts data are from Mahoney et al. (1998); the others are from http://georoc.mpch-mainz.gwdg.de/georoc/Entry.html. (b) Ce/Y–Zr/Nb discrimination diagram (Deniel, 1998) for the Sangxiu basalts. The arrow line indicates the decreasing degrees of partial melting.

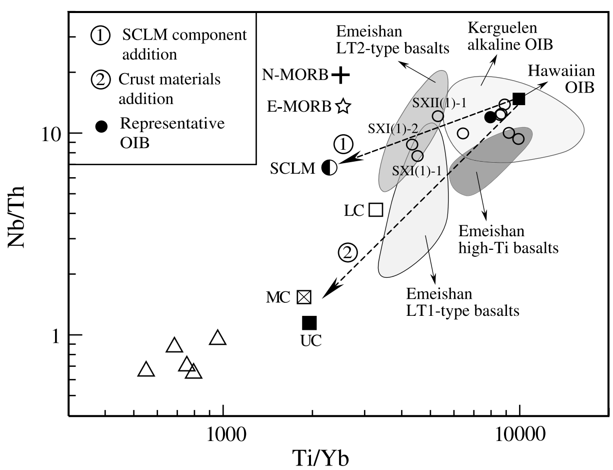

Fig. 13. Plot of Nb/Th vs. Ti/Yb for the Sangxiu basalts. Data for Hawaiian OIB are from Feigenson et al. (1996), Emeishan LT1, LT2-type and high-Ti basalts data are from Xiao et al. (2004), the others are same as Figs. 5 and 7b. Sample symbols as in Fig. 4. Note that all the Sangxiu basalt samples plot between Hawaiian OIB and sub-continental lithospheric mantle/lower crust, the lesser-contaminated samples plot toward the sub-continental lithospheric mantle and/or lower crust (dashed arrow (①), and apart from the trend of sialic crustal materials addition (dashed arrow (②).

The uniform major, trace element geochemical compositions and relatively homogeneous initial $^{87}Sr/^{86}Sr$ ratio require that the Sangxiu felsic volcanic rocks were derived from a relatively homogeneous magma; that is, the assimilation would have to be extremely well mixed into the magma. The εNd(t) values (from −13.39 to −13.05) of the felsic rocks are clearly dissimilar from those of the Sangxiu basalts (from −1.71 to 2.00), suggesting that the first mechanism is unlikely for the Sangxiu felsic volcanic rocks.

In fact, the Nd isotopic compositions of the Sangxiu felsic volcanic rocks are close to those of para-metamorphic rocks (εNd(t) = −11.3 to −20.3, Yang and Jin, 2001) of the Nyalam Group in the Himalaya, and their Nd depleted mantle model age (T_{DM} = 1892–1939 Ma, Table 2) is consistent with the zircon SHRIMP age data that represent the ages of formation of the protoliths of basic granulite in the Higher Himalayan crystallines (1.99±0.3 Ga) and of Nyalam Group Makalu complex (2.1–2.5 Ga), and additionally the zircon SHRIMP age of orthogneiss in Lhagoi Kangri complex (1.86–1.91 Ga) representing the emplacement age of the granite (China Geological Survey, 2004), suggests that the Sangxiu felsic rocks are petrogenetically related to ensialic crust. This is also supported by SHRIMP age data of inherited zircon and overgrowth rims in these felsic rocks (Zhu et al., 2005). From the clear partial melting trend of the felsic lava samples (Fig. 10h–n), and the broad geochemical similarities between the felsic volcanic rocks and those of the middle and upper crust (Figs. 5b and 6b), it is most probable that the Sangxiu felsic rocks were generated by the anatexis of ensialic continental crust.

Experimental results show that dehydration melting of hornblende-bearing granitoids in the shallow crust ($P \leq 4$ kbar, at the depths of 15 km or less) is a likely origin for high-silica metaluminous A-type granites (Patino Douce, 1997). To attain the required melting temperature (> 900 °C) in shallow levels of the crust requires heat and/or mass transfer from mantle-derived, hot basaltic magmas for the origin of A-type rocks. Thus, A-type magmas are usually generated in noncompressive tectonic regimes, such as extension or rifting environments, where the crust tends to be thin and magmatic advection of heat can approach rise in the crust to shallow levels. Such a model for A-type magmas seems applicable to the Sangxiu felsic magmas, in which the heat required for the anatexis of ensialic continental crust can be supplied by plume-derived, hot basaltic magmas from the mantle.

5.6. Implications

The Rajmahal Traps on eastern margin of India, to the south of the outcrop of the Sangxiu volcanic rocks have

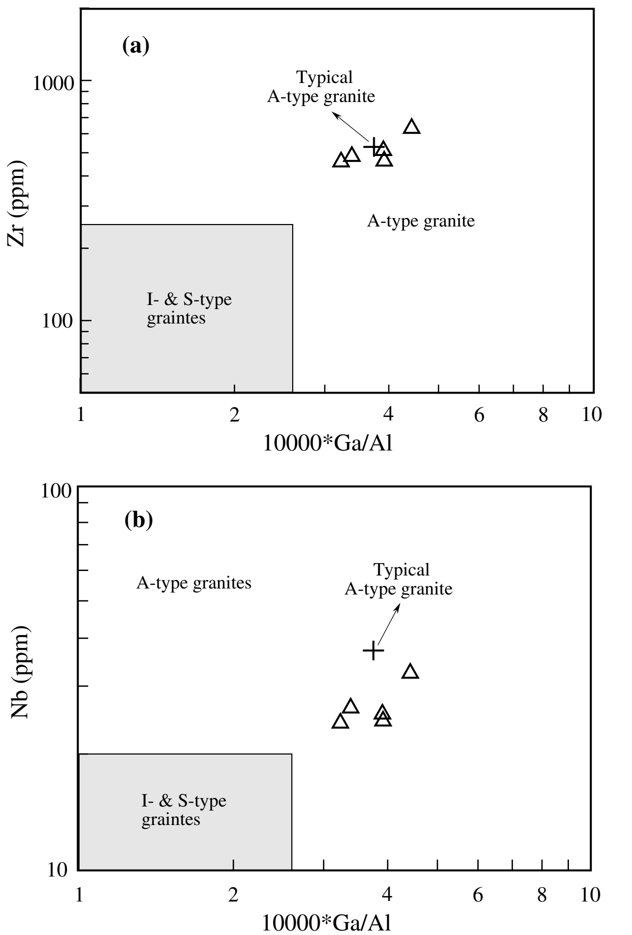

Fig. 14. Plots of the Sangxiu felsic rocks in Zr vs. 10,000 Ga/Al, Nb vs. 10,000 Ga/Al diagrams of Whalen et al. (1987) showing affinity of A-type granite. The typical A-type granite data are from Whalen et al. (1987).

been attributed to early activity of the Kerguelen hotspot (Kent et al., 2002), and the track of Kerguelen hotspot since 120 Ma (Fig. 1b) has been traced from the Rajmahal Traps via the Ninetyeast Ridge to the Kerguelen hotspot in the southern Indian Ocean (Gaina et al., 2002; O'Neill et al., 2003).

The Sangxiu basalts are found to be geochemically and isotopically similar to the basalts of Rajmahal, Ninetyeast Ridge and Kerguelen Island. The volume of the Sangxiu volcanic rocks corresponds to that of the Bunbury basalts in southwestern Australia and Rajmahal basalts in northeastern India (Coffin et al., 2002). On the tectonic reconstruction of Gondwana ca. 130 Ma, based on palaeomagnetism (Fig. 15) the Sangxiu volcanic rocks plot near the southwestern margin of Australia. The age of Sangxiu volcanism (133±3.0 Ma) is close to that of the Bunbury basalt in Western Australia (132.2±0.3 Ma, Coffin et al., 2002). Both of these ages are earlier than the age of Rajmahal basalt (118 Ma, Coffin et al., 2002). It is relatively straightforward to explain similar geochemical characteristics, age of eruption and tectonic location between the Sangxiu basalts and the products of Kerguelen hotspot-related volcanism (e.g. basalts in eastern India, the Ninetyeast Ridge, Kerguelen and southwestern Australia) is that the Sangxiu volcanic rocks were probably generated above the Kerguelen hotspot at ∼133 Ma. Like the Bunbury basalt, the small volume of the Sangxiu volcanic rocks can be ascribed to early activity of Kerguelen hotspot also represented by the Rajmahal basalt (Frey et al., 1996; Coffin et al., 2002; Ingle et al., 2002b). Sangxiu volcanism in the Tethyan Himalaya provides evidence for early activity of the Kerguelen hotspot, extending much farther to the north and northeast, as proposed by Mahoney et al. (2002) and O'Neill et al. (2003).

In addition, ages of the Sangxiu volcanism (133±3.0 Ma) and the Bunbury basalt (132.2±0.3 Ma) are both close to the age of the oldest magnetic anomalies off southwestern Australia (132 Ma, Royer and Coffin, 1992), which become younger to the south along the western coast of Australia (Ingle et al., 2002b). These relationships allow us to suggest that Sangxiu volcanism and Bunbury basaltic volcanism may represent the initial stage of the separation of northeastern Greater India from southwestern Australia.

6. Conclusions

1. The Sangxiu basalts are geochemically similar to the Emeishan high-Ti basalts, and the associated felsic volcanic rocks share most of the geochemical features of A-type granites. The Sangxiu volcanic rocks are interpreted as having been emplaced in a continental rift setting.
2. The Sangxiu basalts were derived from an OIB-type mantle source with discernable contributions from subcontinental lithospheric mantle, the magmas may have formed as a result of the infiltration of plume-derived melts into the base of lithosphere in a continental rift setting, and the felsic volcanic rocks were probably generated by the anatexis of ensialic continental crust.

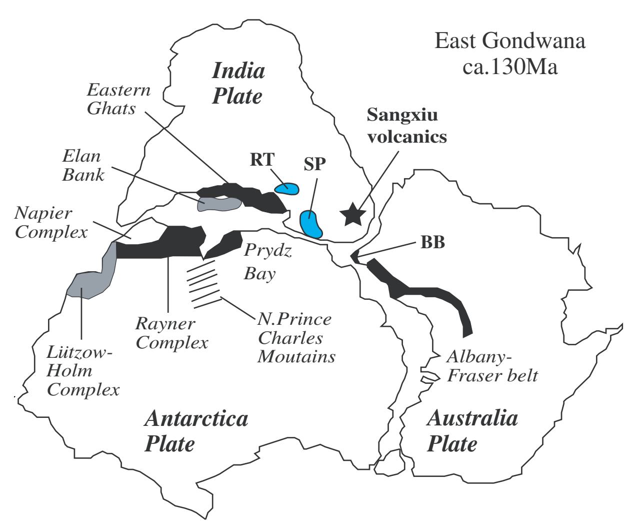

Fig. 15. Generalized plate tectonic reconstruction prior to complete breakup between West Australia, East Antarctica and eastern Greater India ca. 130 Ma (after from Ingle et al., 2002b), showing the positions of the Sangxiu volcanic rocks (black star) in northeastern Greater India, and the Bunbury basalts (BB) in northwestern Australia, Rajmahal Traps (RT) and Shillong Plateau (SP) in eastern India.

3. The similar geochemical characteristics, erupted age and tectonic location between the Sangxiu basalts and the products of Kerguelen hotspot-related volcanism allow us to suggest that the Sangxiu volcanism maybe considered as a consequence of interaction between Kerguelen hotspot and lithosphere of northeastern margin of Greater India at ~133 Ma, and may represent the initial stage of the separation of northeastern Greater India from southwestern Australia.

Acknowledgements

The authors would like to thank Prof. Kazunori Arita and the HKT19 workshop for help during the conference. Comments and discussions provided by Prof. Xu Jifeng, Chung Sun-Lin, Chen Zhiliang, Yu Rulong and Dr Iain D. B. Ross were very helpful in improving and clarifying an early manuscript. We are deeply grateful to Dr Niu Yaoling and an anonymous reviewer for the constructive, valuable comments and suggestions on the manuscript. This study benefited from financial support by the China 973 Program (2002CB412609), NSFC project (40503005), the Integrated Study of Basic Geology in the Blank Area of Southern Tibet (200313000025).

References

Allegre, C.J., Minster, J.F., 1978. Quantitative models for trace element behavior in magmatic process. Earth and Planetary Science Letters 38, 1–25.

Bacon, C.R., Druitt, T.H., 1988. Compositional evolution of the zoned calcalkaline magma chamber of Mount Mazama, Crater Lake, Oregon. Contributions to Mineralogy and Petrology 98, 224–256.

Bienvenu, P., Bougault, H., Joron, M., Dmitriev, L., 1990. MORB alteration: rare-earth element/non-rare earth hygromagmaphile element fractionation. Chemical Geology 82, 1–14.

Bonin, B., 1996. A-type granite ring complex: mantle origin through crustal filters and the anorthosite-rapakivi magmatism connection. In: Demaiffe, D. (Ed.), Petrology and Geochemistry of Magmatic Suites of Rocks in the Continental and Oceanic Crusts. Université Libre de Bruxelles, Royal Museum for Central Africa, Tervuren, pp. 201–218.

Bullen, T.D., Clynne, M.A., 1990. Trace element and isotopic constraints on magmatic evolution at Lassen volcanic center. Journal of Geophysical Research 95, 19671–19691.

Bureau of Geology and Mineral Resources of Xizang Autonomous Region, 1993. Regional Geology of Xizang (Tibet) Autonomous Region. Geological Publishing House, Beijing, pp. 449–450 (in Chinese with English abstract).

Cheng, Q., Park, K.H., Macdougall, J.D., Zindler, A., Lugmair, G.W., Hawkins, J., Lonsdale, P., Staudigel, H., 1987. Isotopic evidence for a hot spot origin of the Louisville seamount chain. AGU monograph 43. In: Keating, B., Fryer, P., Batiza, R., Boechlert, G. (Eds.), Seamounts, Island and Atolls. American Geophysical Union, Washington, DC, pp. 283–296.

China Geological Survey, 2004. Results and progress of regional geological survey: the Himalaya belt. Geological Bulletin of China 23, 27–39 (in Chinese).

Coffin, M.F., Pringle, M.S., Duncan, R.A., Gladczenko, T.P., Storey, M., Müller, R.D., Gahagan, L.A., 2002. Kerguelen hotspot magma output since 130 Ma. Journal of Petrology 43, 1121–1139.

Condie, K.C., 1986. Geochemistry and tectonic setting of early Proterozoic superacrustal rocks in the southwestern United States. Journal of Geology 94, 845–864.

Condie, K.C., Bonnie, A.F., Kerrich, R., 2002. The 1.75-Ga Iron King Volcanics in west-central Arizona: a remnant of an accreted oceanic plateau derived from a mantle plume with a deep depleted component. Lithos 64, 49–62.

Cox, K.G., 1972. The Karoo volcanic cycle. Journal of the Geological Society, London 128, 311–336.

Deniel, C., 1998. Geochemical and isotopic (Sr, Nd, Pb) evidence for plume-lithosphere interaction in the genesis of Grande Comore magmas (Indian Ocean). Chemical Geology 144, 281–303.

Duncan, R.A., 2002. A time frame for construction of the Kerguelen Plateau and Broken Ridge. Journal of Petrology 43, 1109–1119.

Feigenson, M.D., Patino, L.C., Carr, M.J., 1996. Constraints on partial melting imposed by rare earth element variations in Mauna Kea basalts. Journal of Geophysical Research 101, 11815–11829.

Frey, F.A., McNaughton, N.J., Nelson, D.R., Delaeter, J.R., Duncan, R.A., 1996. Petrogenesis of the Bunbury Basalt, western Australia: interaction between the Kerguelen plume and Gondwana lithosphere? Earth and Planetary Science Letters 144, 163–183.

Gaina, C., Müller, R.D., Brown, B., Ishihara, T., 2002. Microcontinent formation around Australia. In: Hillis, R., Müller, R.D. (Eds.). The Evolution and Dynamics of the Australian Plate. Geological Society of Australia Special Publication 22, 399–410.

Garzanti, E., Le Fort, P., Sciunnach, D., 1999. First report of lower Permian basalts in south Tibet: tholeiitic magmatism during break-up and incipient opening of Neotethys. Journal of Asian Earth Sciences 17, 533–546.

Grove, T.L., Donnelly-Nolan, J.M., 1986. The evolution of young silicic lavas at Medicine Lake Volcano, California: implications for the origin of compositional gaps in calc-alkaline series lavas. Contributions to Mineralogy and Petrology 92, 281–302.

Guffanti, M., Clynne, M.A., Muffler, L.J.P., 1996. Thermal and mass implications of magmatic evolution in the Lassen volcanic region, California, and constraints on basalt influx to the lower crust. Journal of Geophysical Research 101, 3001–3013.

Ingle, S., Weis, D., Doucet, S. Mattielli, N., 2003. Hf. Isotope constraints on mantle sources and shallow-level contaminants during Kerguelen hotspot activity since ~120 Ma. Geochemistry, Geophysics, Geosystems 4(8), doi:10.1029/2002GC000482.

Ingle, S., Weis, D., Frey, F.A., 2002a. Indian continental crust recovered from Elan Bank, Kerguelen Plateau (ODP Leg 183, Site 1137). Journal of Petrology 43, 1241–1257.

Ingle, S., Weis, D., Scoates, J., Frey, F., 2002b. Relationship between the early Kerguelen plume and continental flood basalts of the paleo-eastern Gondwanan margins. Earth and Planetary Science Letters 197, 35–50.

Jiang, X.S., Yan, Y.J., Pan, G.T., Liao, Z.L., Zhu, D.C., 2003. Sedimentary environment of the late Jurassic Weimei formation in the southern Tibetan Tethys. Geological Bulletin of China 22, 900–907 (in Chinese with English abstract).

Johnson, B.D., Powell, C.M., Veevers, J.J., 1976. Spreading history of the eastern Indian Ocean and greater India's northwards flight from Antarctic and Australia. Geological Society of American Bulletin 87, 1560–1566.

Kamenetsky, V.S., Everard, J.L., Crawford, A.J., Varne, R., Eggins, S.M., Lanyon, R., 2000. Enriched end-member of primitive MORB melts: petrology and geochemistry of glasses from Macquarie Island (SW Pacific). Journal of Petrology 41, 411–430.

Kent, R.W., Pringle, M.S., Müller, R.D., Saunders, A.D., Ghose, N.C., 2002. $^{40}Ar/^{39}Ar$ geochronology of the Rajmahal basalts, India, and their relationship to the Kerguelen Plateau. Journal of Petrology 43, 1141–1153.

Larson, R.L., 1977. Early Cretaceous breakup of Gondwanaland off western Australia. Geology 5, 57–60.

Li, Y.H., 1991. Distribution patterns of elements in the ocean: a synthesis. Geochimica et Cosmochimica Acta 55, 3223–3240.

Li, S.G., 1993. Ba–Nb–Th–La diagrams used to identify tectonic environments of ophiolite. Acta Petrologic Sinica 9, 146–157 (in Chinese with English abstract).

Li, X.H., Li, Z.X., Zhou, H.W., Liu, Y., Kinny, P.D., 2002. U–Pb zircon geochronology, geochemistry and Nd isotopic study of Neoproterozoic bimodal volcanic rocks in the Kangdian Rift of south China: implications for the initial rifting of Rodinia. Precambrian Research 113, 135–154.

Lin, P.N., Stern, R.J., Bloomer, S.H., 1989. Shoshonitic volcanism in the northern Mariana arc. 2. Large-ion-lithophile and rare earth element abundances: evidence for the source of incompatible element enrichments in intra-oceanic arcs. Journal of Geophysical Research 94, 4497–4514.

Liu, Y., Liu, H.C., Li, X.H., 1996. Simultaneous and precise determination of 40 trace elements in rocks samples using ICP-MS. Geochimica 26, 552–558 (in Chinese with English abstract).

Ludden, J.N., Thompson, G., 1978. Behavior of rare earth elements during submarine weathering of tholeiitic basalts. Nature 274, 147–149.

Mahoney, J.J., Frei, R., Tejada, M.L.G., Mo, X.X., Leat, P.T., Nägler, T.F., 1998. Tracing the Indian Ocean mantle domain through time: isotopic results from old western Indian, East Tethyan, and South Pacific seafloor. Journal of Petrology 39, 1285–1306.

Mahoney, J.J., Duncan, R.A., Khan, W., Gnos, E., McCormick, G.R., 2002. Cretaceous volcanic rocks of the south Tethyan suture zone, Pakistan: implications for the Reunion hotspot and Deccan Traps. Earth and Planetary Science Letters 203, 295–310.

McDonough, W.F., 1990. Constraints on the composition of the continental lithospheric mantle. Earth and Planetary Science Letters 101, 1–18.

Meschede, M., 1986. A method of discriminating between different type of mid-ocean ridge basalts and continental tholeiites with the Nb–Zr–Y diagram. Chemical Geology 56, 207–218.

Niu, Y.Y.L., Regelous, M., Wendt, I.J., Batiza, R., O'Hara, M.J., 2002. Geochemistry of near-EPR seamounts: importance of source vs. process and the origin of enriched mantle component. Earth and Planetary Science Letters 199, 327–345.

O'Neill, C., Müller, D., Steinberger, B., 2003. Geodynamic implications of moving Indian Ocean hotspots. Earth and Planetary Science Letters 215, 151–168.

Pan, G.T., Ding, J., Yao, D.S., Wang, L.Q., Luo, J.N., Yan, Y.J., Yong, Y.Y., Zheng, J.K., Liang, X.Z., Qin, D.H., Jiang, X.S., Wang, Q.H., Li, R.S., Geng, Q.R., Liao, Z.L., Zhu, D.C., Yu, R.L., 2004. Geological Map of Qinghai-Xizang (Tibetan) Plateau and Adjacent Areas (1:1500000). Chengdu Cartographic Publishing House, Chengdu.

Patino Douce, A.E., 1997. Generation of metaluminous A-type granites by low-pressure melting of calc-alkaline granitoids. Geology 25, 743–746.

Pearce, J.A., 1983. Role of the sub-continental lithosphere in magma genesis at active continental margins. In: Hawkesworth, C.J., Norry, M.J. (Eds.), Continental Basalts and Mantle Xenoliths. Shiva, Nantwich, pp. 230–249.

Pearce, J.A., Harris, N.B.W., Tindle, A.G., 1984. Trace element discrimination diagrams for the tectonic interpretation of granitic rocks. Journal of Petrology 25, 956–983.

Roberts, M.P., Clemens, J.D., 1993. Origin of high-potassium, calcalkaline, I-type granitoids. Geology 21, 825–828.

Rollinson, H.R., 1993. Using Geochemical Data: Evaluation, Presentation, Interpretation. Longman, New York, p. 352.

Royer, J.Y., Coffin, M.F., 1992. Jurassic to Eocene plate tectonic reconstructions in the Kerguelen Plateau region. In: Wise, S.W., JrJr, Schlich, R., et al. (Eds.), Proceedings of the Ocean Drilling Program, Scientific Results 120. Ocean Drilling Program, College Station, TX, pp. 917–928.

Rudnick, R.L., Gao, S., 2003. The composition of the continental crust. In: Rudnick, R.L. (Ed.), The Crust. In: Holland, H.D., Turekian, K.K. (Eds.), Treatise on Geochemistry, vol. 3. Elsevier, Oxford, pp. 1–64.

Sciunnach, D., Garzanti, E., 1997. Detrital chromian spinels record tectono-magmatic evolution from Carboniferous rifting to Permian spreading in Neotethys (India, Nepal and Tibet). In: Messiga, B., Tribuzio, R. (Eds.). From rifting to drifting in present-day and fossil ocean basins. Ofioliti 22, 101–110.

Staudigel, H., Plank, T., White, B., Schmincke, H.U., 1996. In: Bebout, G.E., Scholl, S.W., Kirby, S.H., Platt, J.P. (Eds.), Geochemical Fluxes During Seafloor Alteration of the Basaltic Upper Oceanic Crust: DSDP Sites 417 and 418. American Geophysical Union, Washington, DC, pp. 19–38.

Sun, S.S., McDonough, W.F., 1989. Chemical and isotope systematics of oceanic basalts: implications for mantle composition and processes. In: Saunders, A.D. (Ed.). Magmatism in Ocean Basins. Geological Society Publication 42, 313–345.

Team of Integrated General Investigation, 1979. Bureau of Geology and Mineral Resources of Xizang Autonomous Region. Regional Geological Report (1:1,000,000) for Lhasa, P.R.C. unpublished (in Chinese).

Team of Regional Geological Survey, 1994. Regional geological report (1:200,000) for Nagarze-Zedang County, P.R.C. (unpublished). Bureau of Geology and Mineral Resources of Shanxi Province (in Chinese).

Tepper, J.H., Nelson, B.K., Bergantz, G.W., Irving, A.J., 1993. Petrology of the Chilliwack batholith, North Cascades, Washington: generation of calc-alkaline granitoids by melting of mafic lower crust with variable water fugacity. Contributions to Mineralogy and Petrology 113, 333–351.

Tomlinson, K.Y., Hughes, D.J., Thurston, P.C., Hall, R.P., 1999. Plume magmatism and crustal growth at 2.9 to 3.0 Ga in the Steep Rock and Lumby Lake area, western Superior Province. Lithos 46, 103–136.

Turner, S.P., Foden, J.D., Morrison, R.S., 1992. Derivation of some A-type magmas by fractionation of basaltic magma: an example from the Padthaway Ridge, South Australia. Lithos 28, 151–179.

Veevers, J.J., McElhinny, M.W., 1976. The separation of Australia from other continents. Earth Science Review 12, 139–159.

Wang, G.H., Liang, D.Y., Liu, W.C., Dong, W.T., Wang, S.H., 2000. Extensional movement and extending action in southern Tibet since Hercynian. Geoscience 14, 133–139 (in Chinese with English abstract).

Whalen, J.B., Currie, K.L., Chappell, B.W., 1987. A-type granites: geochemical characteristics, discrimination and petrogenesis. Contributions to Mineralogy and Petrology 95, 407–419.

Winchester, J.A., Floyd, P.A., 1977. Geochemical discrimination of different magma series and their differentiation products using immobile elements. Chemical Geology 20, 325–342.

Xiao, L., Xu, Y.G., Mei, H.J., Zheng, Y.F., He, B., Pirajno, Franco, 2004. Distinct mantle sources of low-Ti and high-Ti basalts from the western Emeishan large igneous province, SW China: implications for plume-lithosphere interaction. Earth and Planetary Science Letters 228, 525–546.

Xu, Y.G., 1999. Basaltic magmatism in continental extensional setting: nature and dynamic process. In: Zheng, Y.F. (Ed.), Chemical Geodynamics. Science Press, Beijing, pp. 119–167 (in Chinese).

Yang, X.S., Jin, Z.M., 2001. Studies on Rb–Sr and Sm–Nd isotope of Yadong Leucogranite in Tibet: constraint on its age and source material. Geological Review 47, 294–300 (in Chinese with English abstract).

Yu, G.M., Wang, C.S., 1990. Sedimentary Geology of the Xizang (Tibet) Tethys. Geological Publishing House, Beijing, pp. 10–49 (in Chinese with English abstract).

Zhong, H.M., Xia, J., Tong, J.S., Lu, R.K., Li, Y.H., Yu, X.J., Huang, J., 2003. Regional Geological Report (1:250,000) for Luoza County, P.R.C. (unpublished) (in Chinese).

Zhu, D.C., Pan, G.T., Mo, X.X., Wang, L.Q., Liao, Z.L., Jiang, X.S., Geng, Q.R., 2005. SHRIMP U–Pb zircon dating for the dacite of the Sangxiu formation in the central segment of Tethyan Himalaya and its implications. Chinese Science Bulletin 50, 563–568.